

Evaluation of Seismic Design Parameters for Modular Metal Buildings in High Seismic Zones

Mohammad T. Nikoukalam¹, Shahabeddin Torabian², Benjamin W. Schafer³

ABSTRACT

The objective of this paper is to evaluate the seismic design parameters for modular metal building systems in high seismic zones in the United States using the FEMA P695 methodology. Modular metal buildings, commonly used for large open spaces such as warehouses and data centers, combine traditional built-up tapered steel frames with intermediate gravity-only columns. A suite of archetype buildings with varying spans, heights, and numbers of modules was developed in collaboration with industry and analyzed using nonlinear static and dynamic procedures. High-fidelity shell finite element models, validated against component and shake table tests, capture key failure modes including local and global buckling. Results from pushover and quasi-static cyclic analyses were used to calibrate nonlinear single-degree-of-freedom models for subsequent incremental dynamic analyses against the FEMA P695 earthquake suite. The study demonstrates that modular metal buildings designed with a response modification factor $R = 3.5$ meet the FEMA P695 collapse performance criteria, provided that lateral bracing systems are designed to meet both strength and stiffness requirements of AISC 360. Buildings using traditional strength-only bracing exhibited limited ductility due to premature column buckling, whereas AISC-compliant bracing achieved stable post-peak response and improved collapse margins. A collapse drift limit of 6% is proposed based on system flexibility and observed behavior. The findings confirm the adequacy and applicability of current ASCE 7 Ordinary Moment Frame provisions for modular metal building systems, with important implications for design practice in high-seismic regions.

KEYWORDS

Metal buildings, seismic performance, non-linear, incremental dynamic analysis, fragility

1. INTRODUCTION

Metal building systems in the U.S. typically consist of I-shaped structural steel frames built-up from plate and tapered (particularly in depth) to meet dominant demands, secondary cold-formed steel purlins and girts connecting from frame to frame, diagonal rod bracing to provide diaphragm and cross-frame stiffness, and finished with walls of either steel sheeting or tilt-up concrete panels, and roofs of through-fastened or standing seam metal panels. For long-span metal buildings it is common to support the main frame periodically with gravity columns – creating a

¹ Mohammad T. Nikoukalam, PhD, PE, Consulting Engineer, Simpson Gumpertz & Heger Inc., Washington DC, United States, Email: mtnikoukalam@sgh.com

² Shahabeddin Torabian, PhD, PE, SE, Senior Project Manager, Simpson Gumpertz & Heger Inc., Washington DC, United States, Associate Scientist, Department of Civil and Systems Engineering, Johns Hopkins University, Baltimore, MD, United States, Email: storabian@sgh.com (Corresponding)

³ Benjamin W. Schafer, PhD, PE, Consulting Principal, Simpson Gumpertz & Heger Inc., Washington DC, United States, Willard and Lillian Hackerman Professor, Department of Civil and Systems Engineering, Johns Hopkins University, Baltimore, MD, United States, Email: schafer@jhu.edu

34 “modular” metal building system – as opposed to shorter span systems without interior gravity
35 columns known as “clear-span” metal buildings. It is common to utilize non-compact and slender
36 sections within the tapered main frames to provide sufficient stiffness and necessary strength. For
37 seismic design (in the frame direction) metal building systems are typically categorized as
38 Ordinary Moment Frames (OMF) and thus are only required to meet the design provisions of AISC
39 360 (AISC, 2016). Metal building systems have commonly performed well in earthquakes, but
40 there has been keen interest over the last 20 years to better understand the seismic design of these
41 systems (Uang et al., 2011; M. D. Smith, 2013; Jerry Hatch, 2014).

42 In particular, the experimental work led by Uang at the University of California, San Diego
43 (UCSD) has provided important benchmarks for predicting the performance of metal building
44 systems and components. Quasi-static cyclic tests on a 20 ft × 60 ft [6.1 m × 18.3 m] clear-span
45 primary frame demonstrated elastic behavior up to approximately 2.5% drift, beyond which
46 stiffness and strength degraded due to lateral-torsional buckling (LTB) in the column (Hong and
47 Uang, 2006). Cyclic component testing of column-knee-rafter connections demonstrated that large
48 drifts were accompanied by LTB in the rafter between brace points, along with flange local
49 buckling (FLB), and the members could undergo multiple cycles and large drifts (beyond 6%)
50 without fracture, but with strength loss. Comparisons of test results with AISC Design Guide 25 -
51 Frame Design using Web-Tapered Members (Kaehler et al., 2011) demonstrated that accurate
52 prediction of LTB capacity requires explicit consideration of bracing conditions.

53 Finally, full-scale shake table testing of three clear-span metal buildings to evaluate seismic
54 performance under varying configurations, including light and heavy wall cladding and
55 mezzanines was performed at UCSD (Figure 1) (Uang et al., 2011; M. D. Smith, 2013). The tests
56 demonstrated significant system overstrength, with all specimens remaining stable up to 150% of
57 the Imperial Valley ground motion scaled to ASCE 7 (ASCE, 2016) design earthquake (DE) levels
58 – and one specimen tested up to 300% DE without collapse (note, maximum considered earthquake
59 levels, or MCE are 150% DE). Maximum drift ratios experienced across the specimens varied
60 from 3.5% to 5.4% and LTB, FLB, and panel zone buckling and yielding were observed in the
61 specimens. The buildings with heavy wall attachments exhibited limit states at earlier drifts than
62 those with light walls. None of the buildings collapsed under the imposed excitations and the tests
63 stopped due to other experimental limitations on the shake table.

64 To complement the experimental findings, high-fidelity finite element modeling has become
65 essential for evaluating seismic performance, particularly in utilizing the FEMA P695 procedure
66 (ATC, 2009) to validate seismic response modification coefficients (e.g. R). The second and third
67 authors of this paper were part of a team that developed a peer-reviewed seismic modeling
68 procedure for the seismic performance of clear-span metal buildings shaking in the direction of
69 the main frames (Meimand et al., 2018; Moen et al., 2019). The overall approach utilized a high-
70 fidelity, primarily shell, finite element model of the metal building system to characterize the
71 nonlinear static hysteretic response of the frame and a nonlinear single degree of freedom model
72 to perform the required incremental dynamic analyses (IDA) across a suite of earthquakes to assess
73 the predicted collapse margin ratio. The high-fidelity model incorporated all typical metal building
74 details including flange braces, metal roof panels, and rod bracing and was validated against
75 component testing of the main frame and the shake table tests at UCSD (Moen et al., 2019). The
76 peer-reviewed P695 study confirmed the applicability of the OMF seismic response modification
77 coefficient $R = 3.5$ for both traditional light walls and tilt-up heavy walls for clear-span metal
78 buildings (Meimand et al., 2018; Moen et al., 2019). Highlighted in the overall findings from this

79 work were: (1) clear-span metal building systems are unique in that the gravity and lateral framing
80 systems are combined and member depths and details are influenced prominently by both gravity
81 and lateral demands in the same frame; (2) the period of metal buildings is typically longer than
82 empirical expressions provided in ASCE 7, therefore story drifts (even within the elastic regime)
83 are often greater than conventional steel-frame building systems; and (3) the bracing connected
84 between the purlins or girts and the main frame is critical to stable large lateral deformation
85 response even as global (e.g. lateral-torsional) buckling initiates.



86
87

Figure 1. Assembled specimen on shaking table (M. SD. Smith et al., 2013)

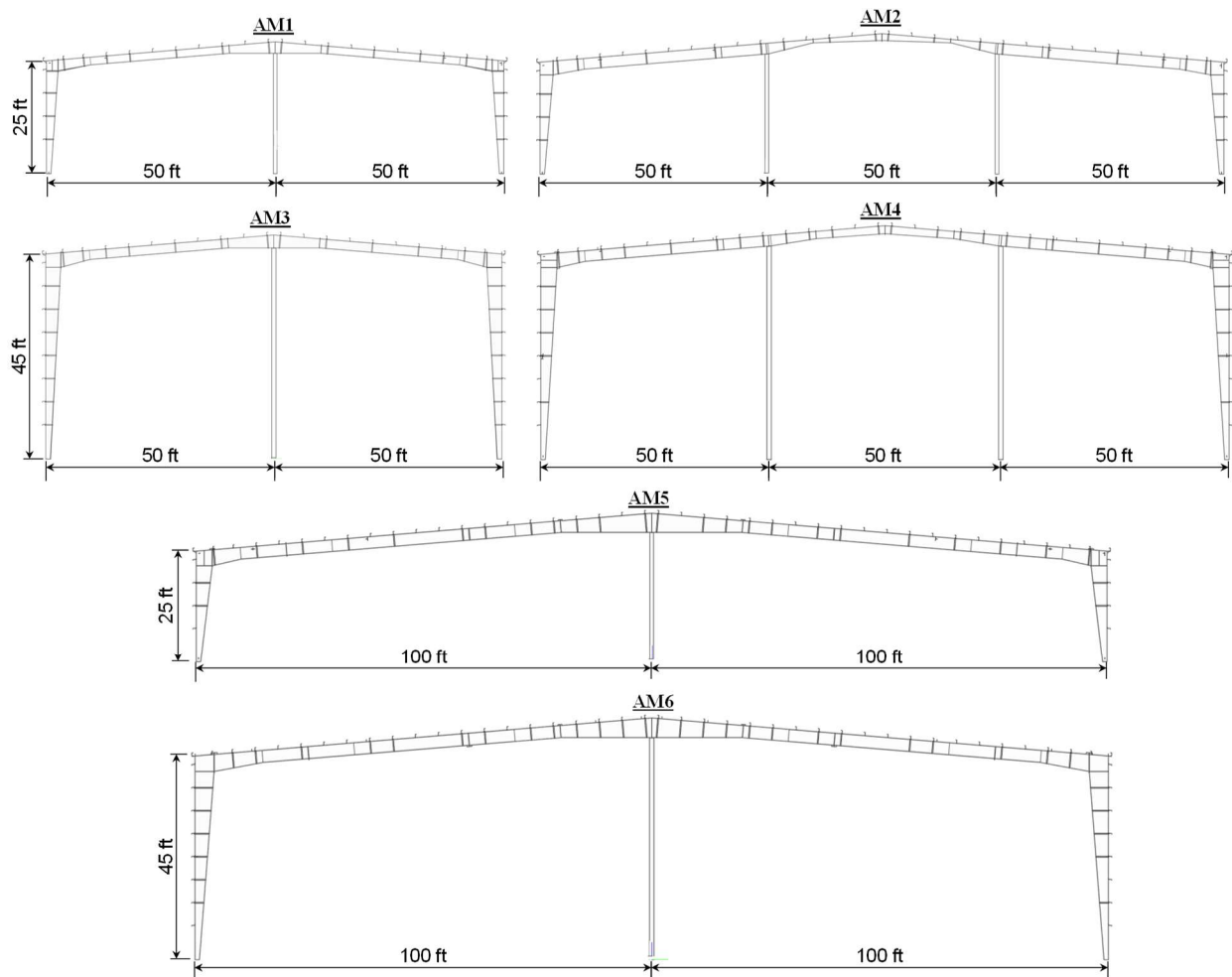
88 Beyond the United States, similar modeling efforts have been undertaken to investigate the
89 seismic performance of both clear-span and modular metal building systems in Canada (Bagatini
90 Cachuço, 2021; Bagatini Cachuco & Yang, 2021) and provide guidance on appropriate seismic
91 response modification coefficients for use in equivalent lateral force procedures in the National
92 Building Code of Canada (NBCC). The analytical framework employed included shell finite
93 element models of components (e.g. the column-knee-rafter segment) in ABAQUS then utilized
94 to calibrate a beam finite element model of the main frame implemented in OpenSees (McKenna
95 et al., 2004). IDA was conducted on the OpenSees model for a suite of earthquake motions relevant
96 to western Canada. The researchers performed a series of trial designs considering different levels
97 of assumed ductility-based seismic force reductions (in Canada overstrength and ductility seismic
98 force reductions are separated into two parts) and concluded that the ductility-based force
99 reductions should be approximately 1.3 for metal buildings in western Canada.

100 The research reported herein uses the framework of Moen et al. (2019) to evaluate the seismic
101 response modification coefficients for modular metal building systems in high-seismic regions in
102 the United States. A series of modular metal building system archetypes are designed in
103 collaboration with industry. A high-fidelity shell finite element model of the archetypes is
104 developed and exercised through modal analysis, geometric and material nonlinear static pushover
105 analysis, and geometric and material nonlinear static cyclic analysis. A nonlinear single degree of
106 freedom surrogate model is calibrated to the high-fidelity model and utilized for IDA across the
107 FEMA P695 earthquake suite. Formal P695 evaluation is performed to assess the adequacy of the

108 assumed seismic response modification coefficients. The scope is limited to modular metal
109 buildings up to 45 ft [13.7 m] in eave height and with roof loads no greater than 20 psf [0.96
110 kN/m²] in high-seismic zones.

111 2. DESIGN OF MODULAR METAL BUILDING ARCHETYPES

112 A critical step in the assessment of seismic performance modification factors per FEMA P695
113 is the development of system archetypes. Previously, for clear-span metal buildings four
114 archetypes covering light and heavy walls and ranges of height-to-span for the main frames
115 consistent with known practice were developed (Moen et al., 2019). For modular metal buildings
116 six archetypes were developed, as summarized in Table 1 and depicted in Figure 2 **Error!**
117 **Reference source not found..** The buildings cover a range of heights and utilize either 2 or 3
118 modules with spans between the interior columns of 50 ft [15.2 m] or 100 ft [30.4 m]. The
119 archetype buildings were designed and detailed by engineers at Metal Building Manufacturers
120 Association (MBMA) member companies using their own internal design, detailing, and
121 optimization software with the parameters defined in Table 1 and Table 2.



122

123

Figure 2. Schematic elevation view of modular archetype buildings

124

Table 1: Metal building archetypes dimensions and design loads

Archetype	H	$N \times \text{Span}$	Bay	V_r
	ft [m]	$N \times \text{ft [m]}$	ft [m]	kip [kN]
AM1	25 [7.6]	2×50 [15.2]	25 [7.6]	17.6 [78.3]
AM2	25 [7.6]	3×50 [15.2]	25 [7.6]	25.6 [118.3]
AM3	45 [13.7]	2×50 [15.2]	25 [7.6]	18.6 [82.7]
AM4	45 [13.7]	3×50 [15.2]	25 [7.6]	26.6 [118.3]
AM5	25 [7.6]	2×100 [30.4]	25 [7.6]	33.8 [150.2]
AM6	45 [13.7]	2×100 [30.4]	25 [7.6]	34.8 [154.8]

125

126

Table 2. Archetype design assumptions

Summary of Demand Side (ASCE 7) Design Assumptions	
Building risk/occupancy category	II
Roof slope	1:12
Roof dead load (psf [Pa])	2.2 [105.3]
Self-weight (psf [Pa])	2.5 [119.7]
Collateral load (psf [Pa])	7 [335.2]
Roof live (reducible) (psf [Pa])	20 [957.6]
Snow load (psf [Pa])	0 [0]
Rain load (psf [Pa])	0 [0]
Wind speed (mph [kph])	110 [177]
Wind exposure category	B
Seismic importance factor	1.0
Seismic design category	D
Site class	D
F_a, F_v	1, 1.7
S_s (g), S_1 (g)	1.5, 0.6
S_{DS}, S_{DI}	1, 0.68
R, Ω_o, C_d	3.5, 2.5, 3
Redundancy factor (ρ)	1.3
Design method	Allowable stress design
Seismic load	Equivalent lateral force procedure
Drift limit	No limit. Exterior walls accommodate frame drift (ASCE 7 Table 12.12-1)
Summary of Capacity Side (AISC 360) Design Assumptions	
Metal building frame	OMF
seismic detailing specifications	Three-plate members, pinned Base, no restriction on member compactness, no restriction on member splice locations, no restrictions on taper, pinch point, belly points, no special design of the panel zone
AISC 341 seismic provisions: overstrength conditions	AISC design guide 16 connection type, design knee connection with $R=1.0$ Use Ω_o forces only for column and base plate axial load including anchor rods and welding.
Material	Specified $F_y = 55$ ksi [379 MPa], $F_u = 70$ ksi [482 MPa]
Welding	AWS D1.8 provisions, no protected zones
Anchor rods	ASTM F1554 A36

127

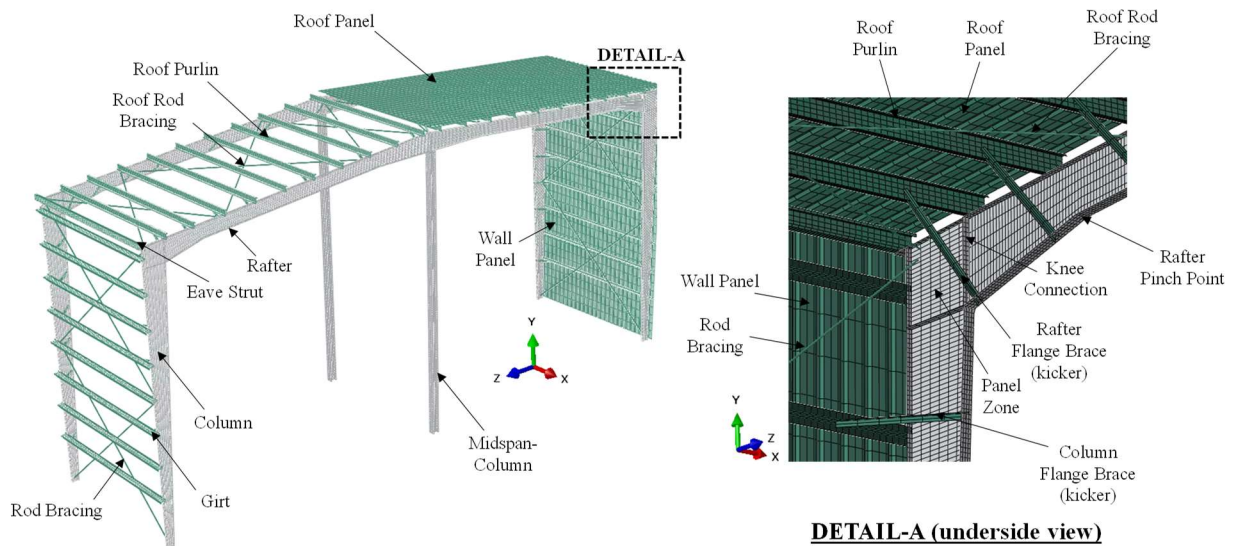
128 To insure more sections of the frames are controlled by seismic demand, snow load
 129 combinations were not included in developing the frame designs because this leads to lower-
 130 weight design (see Moen et al. (2019) for influence of snow loads on seismic designs). To insure

131 realistic secondary member sizes, and eliminate site specificity roof purlins, roof decks,
 132 diaphragms, girts, and lateral braces were designed against the United States average wind load
 133 for components and cladding, which corresponds to a wind speed of 110 mph [177 kph]; however
 134 wind did not control design of the frame members (i.e., seismic controls the lateral demands). The
 135 modular archetype metal buildings are designed for the Design Earthquake (DE) per ASCE 7-16.
 136 The values taken for the spectral response acceleration parameter at short period, S_s , and for the
 137 spectral response acceleration parameter at a period of 1.0, S_1 , are based on recommendations
 138 provided in FEMA P695 (ATC, 2009).

139 3. NUMERICAL MODELLING

140 This section describes the high-fidelity (primarily shell) finite element model used to predict
 141 the nonlinear lateral response of a modular metal building frame. The frame columns and rafters
 142 as well as the purlins, girts, and sheeting are all modeled with shell finite elements (Figure 3).
 143 Therefore, the model is capable of capturing local and global buckling of the rafters and columns,
 144 local, distortional, and global buckling (including stiffness loss) of the purlins and girts, as well as
 145 buckling and yielding of the panel zone. The model does not include consideration of fracture. The
 146 initial modeling protocols, as detailed further below in their current use, were developed for the
 147 study on clear-span metal building frames (Meimand et al., 2018; Moen et al., 2019) and subject
 148 to peer review (see acknowledgments for the peer review team details). The main frame (rafter)
 149 modeling was validated against quasi-static cyclic frame subassembly tests conducted to the AISC
 150 341-10 (AISC, 2010) protocol (Smith et al., 2013). The complete model was validated against
 151 three full-scale shake table tests conducted at UCSD (Uang et al., 2011 and Smith et al., 2013).

152



153

154

Figure 3. High fidelity finite element model

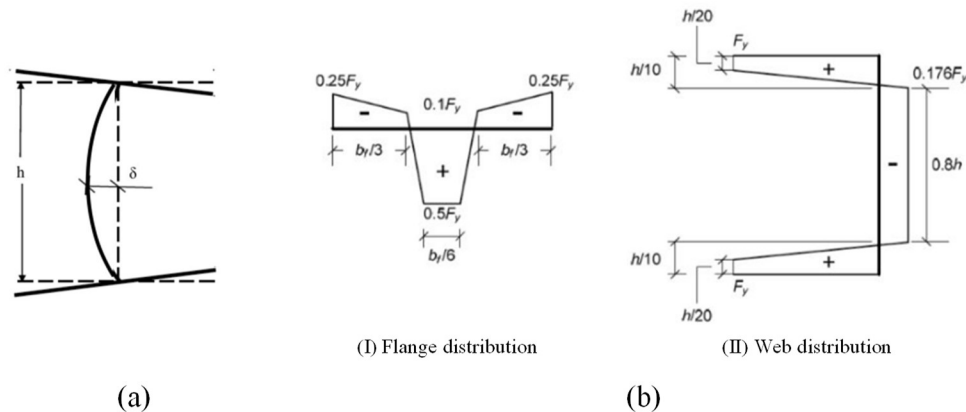
155 All finite element modeling in this study is performed in ABAQUS (Simulia, 2014). Model
 156 generation was automated (MathWorks, 2018) to get all geometrical and material properties of the
 157 archetypes and generate ABAQUS input files. The inputs include rafter and column sizes, tapering,
 158 purlin and girt shapes, roof and wall panel sizes, main frame lateral bracing, lateral rod bracing,
 159 horizontal roof truss diaphragm, and the material properties of all associated parts.

160 The main frame is modeled with 4-node S4R finite strain shell elements in ABAQUS,
 161 following mesh density guidelines defined in Schafer et al. (Schafer et al., 2010), which set a
 162 minimum of 4 nodes per local buckling half-wavelength. The plate-to-plate connections at the
 163 web-to-flange juncture or stiffeners to other elements are provided by common nodes, or tie
 164 constraints, and the welds are not explicitly modeled herein.

165 The pre-tensioned bolts of the end plate connections are not explicitly modeled, but the rafter
 166 (or column) end plate and the knee end plate are modeled to always stay in contact, assuming that
 167 the precompression is not overcome during the simulations.

168 The imperfections are considered as distortional buckling half-wavelength with the maximum
 169 web imperfection of $\delta=h/250$, where h is the depth of the web, as shown in Figure 4(a). A global
 170 out-of-plane sweep in the main frame span of $L/1000$ is also included based on measurements
 171 taken in the UCSD cyclic subassembly tests (Smith, 2013).

172 Thermal self-equilibrating residual stresses are modeled in the main frames with the stress
 173 distributions shown in Figure 4(b). The stress magnitudes are chosen based on the suggestions
 174 from Prawel (Prawel et al., 1974) and Kim (Kim, 2010) for built-up steel members.



175
 176 **Figure 4. Mainframe: (a) cross-sectional geometric imperfection pattern; (b) thermal residual stress**
 177 **pattern (Kim, 2010)**

178 Purlins and girts are also modeled using S4R shell elements, with a cross-section node pattern
 179 extruded along the length. The purlins are connected to the main frames with numerical constraints
 180 that link a group of nodes in the web and the bottom flange of the secondary member to a group
 181 of nodes on the main frame flange. These constraints approximate a typical clip connection. The
 182 girts and purlins are connected to the wall and roof panels by fasteners, where the fastener
 183 connection is modeled as a rigid constraint between coincident nodes using the MPC Beam in
 184 ABAQUS (Simulia, 2014). Initial geometric imperfections and residual stresses from
 185 manufacturing are not considered for any secondary members.

186 Rod braces are modeled with B33 beam elements in ABAQUS, and multi-point constraint
 187 (MPC) connections are used on the web near the top flange. The brace angle cross-sections are
 188 modeled with S4R shell elements, and the brace ends are numerically constrained to node groups
 189 in the main frame flange and the purlin.

190 Wall and roof steel deck sheathing are modeled using shell elements, where sidelaps and
 191 endlaps are assumed to be continuous. Screw-fastened roofs are evaluated in this study, and each

192 panel-to-purlin and panel-to-girt screw connection is modeled with a single-node rigid MPC.

193 Yield stress of 55 ksi [379 MPa] and ultimate stress of 70 ksi [482 MPa] are used for all steel
 194 structural elements. An isotropic-kinematic plasticity model where the von Mises yield surface
 195 both expands and shifts to include residual stresses that remain after elastic unloading (i.e., the
 196 Bauschinger effect) is considered in both static and cyclic models. All secondary structural
 197 elements, including purlins, girts, and lateral braces, are of a yield stress of 50 ksi [345 MPa] and
 198 an engineering strain hardening slope of $0.25\%E$ with isotropic hardening, where E is the elastic
 199 modulus of the steel material.

200 4. ANALYSIS AND EVALUATION OF ARCHETYPE BUILDINGS

201 4.1. Pushover Analysis

202 Prior to performing nonlinear cyclic or dynamic analyses, a pushover analysis of the high-
 203 fidelity metal building model is performed. This analysis is utilized to determine the period-based
 204 ductility parameter (μ_T) and the system overstrength factor (Ω_o) for each archetype per FEMA
 205 P695. Additionally, the pushover analysis helps check the accuracy of the model and identify the
 206 expected failure modes. The pushover response also aids in defining a drift-based collapse limit,
 207 as detailed further in Section 4.4. The model is fully geometric and material nonlinear and therefore
 208 includes all large deformation ($P-\Delta$ and $P-\delta$) effects.

209 Figure 5 provides the static pushover response in terms of base shear versus roof displacement
 210 for all archetype buildings. “Tall buildings” AM3 and AM4 have insufficient ductility for
 211 successful seismic performance. Both suffer greater than 20% strength loss at peak load although
 212 they have sufficient strength (i.e., the peak strength is well in excess of the design strength). The
 213 observed post-peak response for AM3 and AM4 are provided in Figure 5 and Figure 6(a) and (c)
 214 respectively, and in both cases one can observe that the girts are unable to brace the column rafter
 215 and LTB in the column is occurring across multiple brace points. Consultation with the design
 216 engineers resulting in learning that the purlin and girt designs for AM3 and AM4 followed
 217 historical practice of using 2% of the compressive force (or flange force) in sizing the brace. AISC
 218 360 Appendix 6 requires that both strength (often less than 2%) and stiffness be supplied by the
 219 bracing system. In this case, a redesign was required using heavier (thicker) girts to meet the
 220 stiffness requirement.

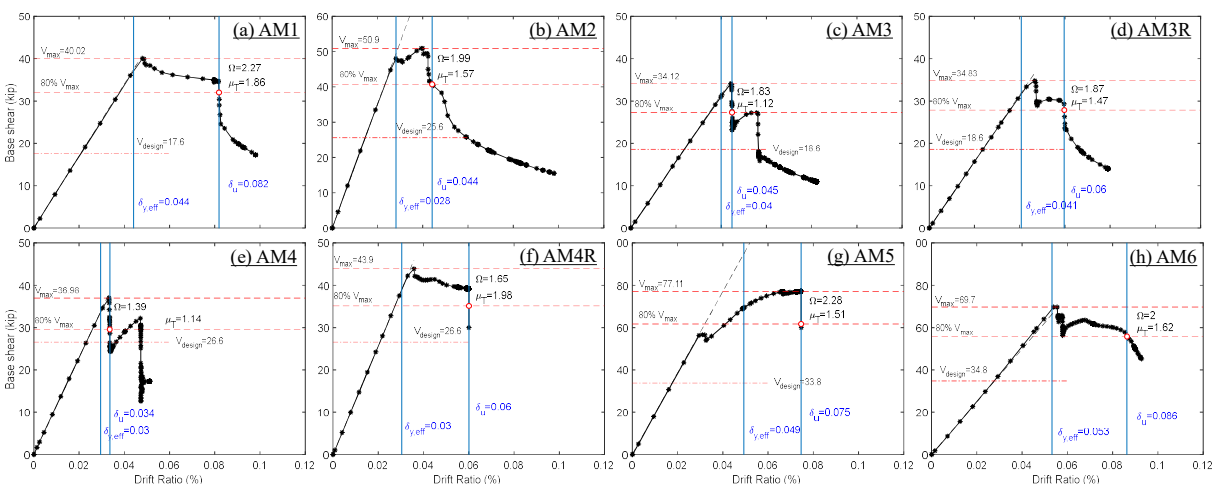
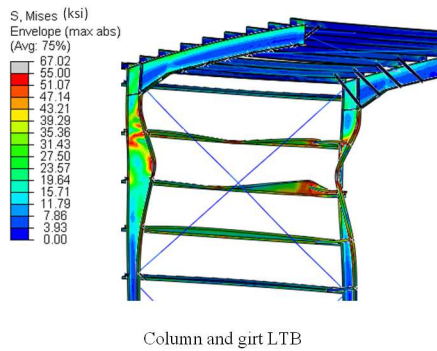
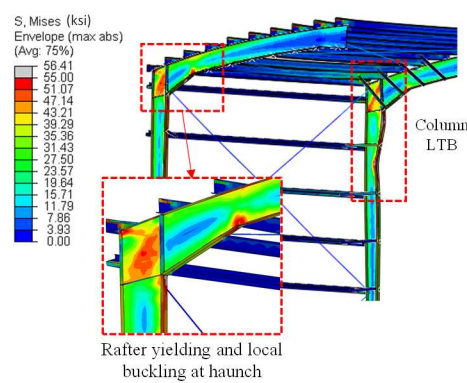


Figure 5. Static pushover curve of archetypes [1kip = 4.448 kN].

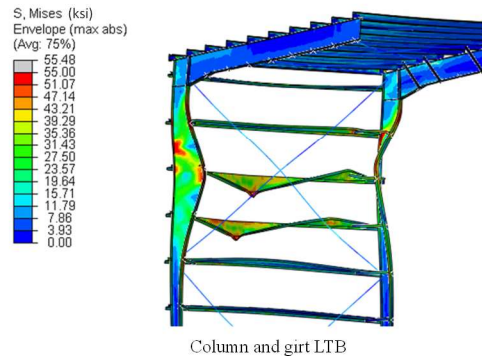
(a) AM3: 4.5% Drift Ratio



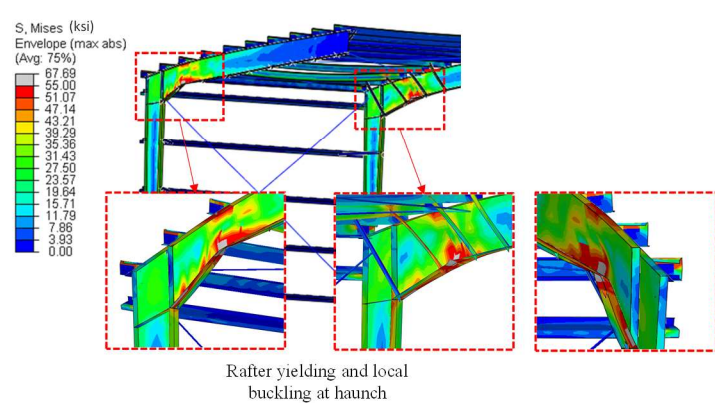
(b) AM3R: 4.7% Drift Ratio



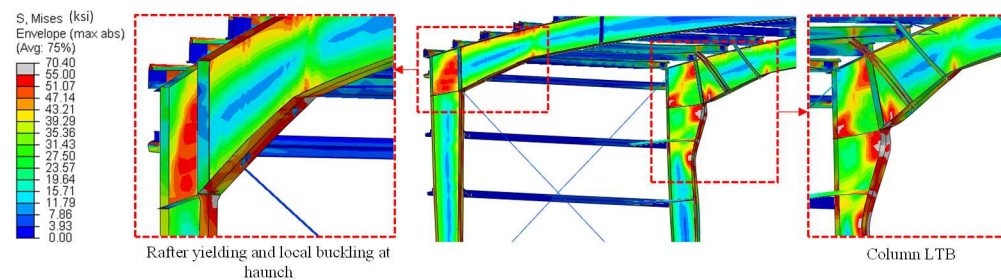
(c) AM4: 3.4% Drift Ratio



(d) AM4R: 3.6% Drift Ratio



(e) AM6: 5.6% Drift Ratio



223

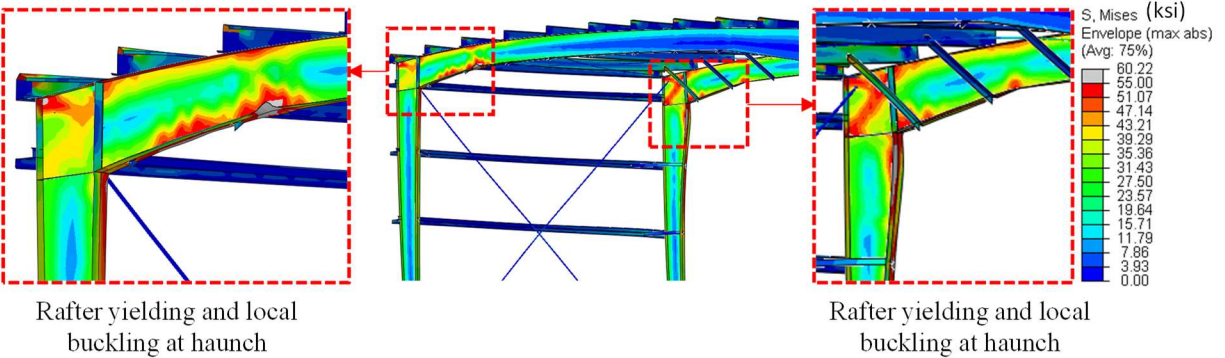
224 **Figure 6. First failure mode in tall buildings (45 ft [13.72 m]): (a) AM3, (b) AM3R, (c) AM4, (d)**
225 **AM4R, (e) AM6 [1ksi = 6.895 MPa]**

226 The performance of the redesigned AM3 and AM4 archetypes, designated as AM3R and
 227 AM4R are provided in Figure 5 and in Figure 6(b) and (d). The overall response of the redesigned
 228 AM3R and AM4R results in adequate post-peak ductility and moves the limit state from LTB in
 229 the column to local buckling and yielding in the rafter. AM6 (the final tall building) was designed
 230 after AM3R and AM4R and also had the bracing provisions of AISC 360 Appendix 6 applied in
 231 its design. Note, AM1, AM2 and AM5 (the shorter buildings) did not have the AISC 360 Appendix
 232 6 bracing provisions applied; however, they still performed well. Figure 5 provides the pushover
 233 response and Figure 7 provides the deformed shape and stress contours for AM1, AM2, and AM5.

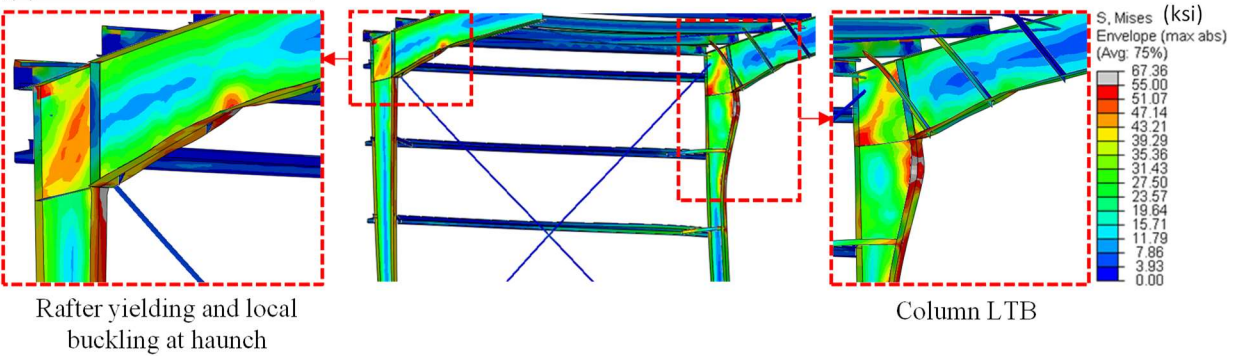
234 The initial limit state is rafter yielding and local buckling at the haunch and detrimental column
 235 LTB does not occur until larger drifts. It is anticipated that similar strength, but improved post-
 236 peak performance is possible in these archetypes if they were to be redesigned to AISC 360
 237 Appendix 6 bracing stiffness and strength provisions; however, given the performance was
 238 adequate as designed, the investigation of the overall performance proceeded without redesign and
 239 reanalysis on these archetypes.

240

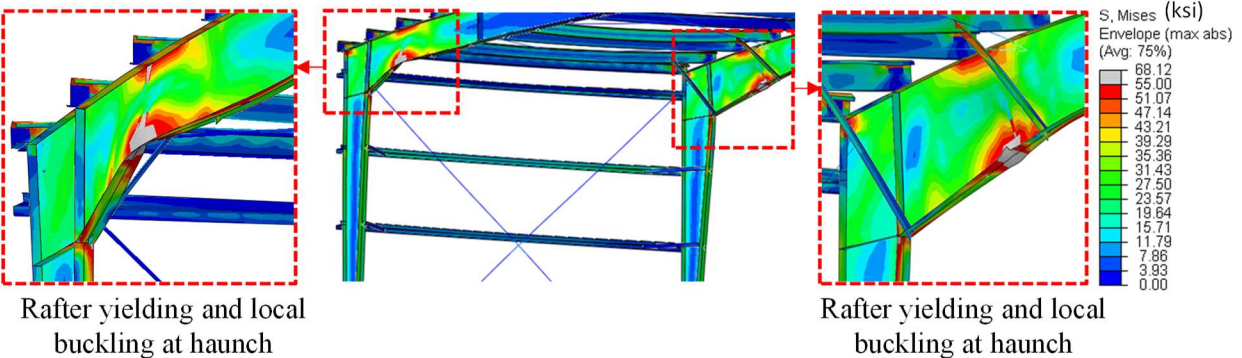
(a) AM1: 4.9% Drift Ratio



(b) AM2: 3.0% Drift Ratio



(c) AM5: 3.3% Drift Ratio



241
 242
 243

Figure 7. First failure mode in short buildings (25 ft [7.62 m]): (a) AM1, (b) AM2, (c) AM5 [1ksi = 6.895 Mpa]

244 Based on the nonlinear static pushover response the resulting system overstrength (Ω_o),
 245 ductility (μ), and period-based ductility (μ_T) for each archetype are summarized in Table 3. The
 246 system overstrength is defined as $\Omega_o=V_{max}/V_{design}$, where V_{max} is the maximum base shear, and
 247 V_{design} is the design base shear, i.e., the lateral demand at the Design Earthquake (DE) level. The
 248 ductility is defined as $\mu=\delta_u/\delta_y$, where δ_u is the ultimate roof drift displacement, i.e., the roof
 249 displacement at $0.8V_{max}$, and δ_y is the yield roof drift displacement, defined as $\delta_y= V_{max}/k_e$, where
 250 k_e is the initial (elastic) stiffness of the building. The period-based ductility is defined as $\mu_T=\delta_u/\delta_{y,eff}$,
 251 where δ_u is the ultimate roof drift displacement, i.e., the roof displacement at $0.8V_{max}$, and $\delta_{y,eff}$ is
 252 the effective yield roof drift displacement, $\delta_{y,eff}$, defined in FEMA P695 as:

$$\delta_{y,eff} = C_o \left[\frac{V_{max}}{W} \right] \left[\frac{g}{4\pi^2} \right] (\max(T, T_1))^2 \quad (1)$$

253
 254 where T is the fundamental period per ASCE 7-16, T_1 is the fundamental period of the building
 255 models computed using eigenvalue analysis (see Section 4.2), W is the seismic weight of the
 256 building, g is the acceleration of gravity, V_{max} is the maximum base shear of the building, and C_o
 257 is the modal coefficient which is 1.0 for a single-story structure like a metal building.

258 **Table 3. Summary of system overstrength (Ω_o), ductility, and period-based ductility (μ_T) factors for each**
 259 **archetype.**

Archetype	Overstrength	Ductility	Period-Based Ductility
	Ω_o	μ	μ_T
AM1	2.27	1.67	1.86
AM2	1.99	1.49	1.57
AM3R	1.87	1.39	1.47
AM4R	1.65	>1.94	>1.98
AM5	2.28	>1.48	>1.51
AM6	2	1.47	1.62
Average	2.01	>1.57	>1.67
Archetypes prior to redesign of bracing stiffness per AISC 360			
AM3	1.83	1.07	1.12
AM4	1.39	1.09	1.14

260
 261 According to Table 3, the calculated overstrength factors are in the range of 1.6 to 2.3.
 262 According to the FEMA P695 procedures, the system overstrength, Ω_o , is calculated as the
 263 maximum of the average from the different performance groups, but not to exceed a maximum
 264 value of $\Omega_o=3.0$. Accordingly, from the archetype analysis summarized in Table 3, the design value
 265 would be set to $\Omega_o=2.0$, governed by the average value of the performance group.

266 The nonlinear static pushover analysis provides a clear examination of the expected limit
 267 states. The sequence of failure modes observed in each archetype is presented in Table 4.

Table 4. Sequence of observed behavior in each archetype

Archetype	Observed Behaviour		Drift (%)	Post-peak Behavior	Drift (%)	Large-drift Behavior
	Drift (%)	First Significant Behavior				
AM1	4.9	Rafter Y and LB	5.1	Rafter and column LTB	8.0	Rafter and PZ Y
AM2	3.0	Rafter Y and LB Column LTB	4.2	Rafter and PZ Y	4.3	Column LTB
AM3R	4.7	Rafter Y and LB Column LTB	4.7	Column LTB	5.8	Rafter and PZ Y
AM4R	3.6	Rafter Y, LB, and LTB	3.8	Rafter LTB purlin LB	6.0	Rafter and PZ Y
AM5	3.3	Rafter Y, LB, and LTB	4.9	Rafter and PZ Y	6.7	Purlin LTB
AM6	5.6	Rafter Y and LB Column LTB	5.8	Rafter and purlin LTB	6.8	Rafter and PZ Y
Archetypes prior to redesign of bracing stiffness per AISC 360						
AM3	4.5	Column and girt LTB	5.6	Rafter and PZ Y	5.6	Column LTB
AM4	3.3	Column LTB	3.4	Girt LTB	4.7	Rafter Y Column LB and LTB

Note: Y: Yielding, LB: Local Buckling, LTB: Lateral-Torsional Buckling, PZ: Panel Zone

269

270

271 Major observations from the nonlinear static response include:

- 272 • In “short” archetypes ($H=25$ ft [7.62 m]), AM1, AM2, and AM5, the post-peak response
273 is primarily dominated by rafter yielding and local buckling at the haunch, followed by
274 rafter span LTB at larger drift ratios in all three archetypes and minor column LTB in AM1
275 and AM2.
- 276 • In tall archetypes (45 ft [13.72 m]) with column lateral bracing designed per the strength-
277 only (2%) method (i.e., AM3 and AM4), the post-peak strength degradation is dominated
278 by severe column LTB (Figure 6(a) and (c)), followed by girt LTB due to the diagonal
279 brace (kicker) force at the location of column lateral braces. The high sensitivity of AM3
280 and AM4 to column LTB results in significantly lower ductility than the other archetypes.
281 These bracing designs do not meet the criteria of AISC 360.
- 282 • In tall archetypes with column lateral bracing designed per AISC 360 (AM3R, AM4R, and
283 AM6), the post-peak strength degradation is primarily dominated by rafter yielding and
284 local buckling at the haunch followed by rafter span or minor column LTB (Figure 6(b),
285 (d), and (e)). The lower sensitivity of AM3R, AM4R, and AM6 to column LTB results in
286 a more stable post-peak response and higher ductility than AM3 and AM4.

287 With these findings it was concluded that application of the OMF criteria in seismic design of
288 metal buildings must adhere to all provisions of AISC 360, including the bracing provisions, and
289 designing of braces for 2% of the compressive force is not sufficient. Therefore, further analysis
290 would only be conducted on AM3R and AM4R. As a result, in the analyses that follows AM3
291 and AM4 are replaced by AM3R and AM4R.

292

293 **4.2. Frequency (Modal) Analysis**

294 The natural periods and mass participation of the modular metal building archetypes are
 295 provided in Table 5. The natural period of the tall archetypes (AM3R, AM4R, and AM6) is
 296 between 2.02 and 2.39 sec., while that of the shorter ones (AM1, AM2, and AM5) ranges from
 297 1.19 to 1.89 sec. The high-fidelity model and the beam element model used in the design agree
 298 strongly, while the empirical equations in ASCE 7-10 (ASCE, 2010) were found to assume far
 299 stiffer response than is typically realized in metal building frames.

300 **Table 5. Summary of the modal analysis results of the high-fidelity models and period evaluation of the**
 301 **archetype buildings per ASCE 7-16 method**

Archetype	mass participation ratio	T_1 (s)	T_{ASCE7} (s)	T_{Design} (s)	$\frac{T_1}{T_{ASCE7}}$	$\frac{T_1}{T_{Design}}$
AM1	0.92	1.44	0.39	1.42	3.67	1.02
AM2	0.99	1.19	0.40	1.20	2.95	0.99
AM3R	0.96	2.02	0.61	1.98	3.31	1.02
AM4R	0.97	1.89	0.62	1.89	3.05	1.01
AM5	0.74	1.53	0.42	1.35	3.67	1.13
AM6	0.93	2.39	0.63	2.24	3.79	1.07

302 T_1 : first period of high fidelity shell finite element model
 303 T_{ASCE7} : estimate period based on ASCE 7-16, Eq. 12.8-7
 304 T_{Design} : period estimate by metal building designer based on beam element approximation
 305

306
 307 **4.3. Cyclic Analysis**

308 The high-fidelity models are used to characterize the quasi-static cyclic response of the
 309 archetypes, including strength and stiffness degradation. Each archetype metal building is
 310 subjected to cyclic horizontal displacements per AISC 341 cyclic loading protocol at the knee
 311 level. The cyclic response is defined as the base shear versus drift ratio in Figure 8. The cyclic
 312 results generally follow the pushover backbone, but some minor cyclic degradation is observed in
 313 the archetypes. The quasi-static cyclic behavior is used to calibrate a non-linear single degree of
 314 freedom (SDOF) model utilized in incremental dynamic analysis and discussed in the following
 315 section.

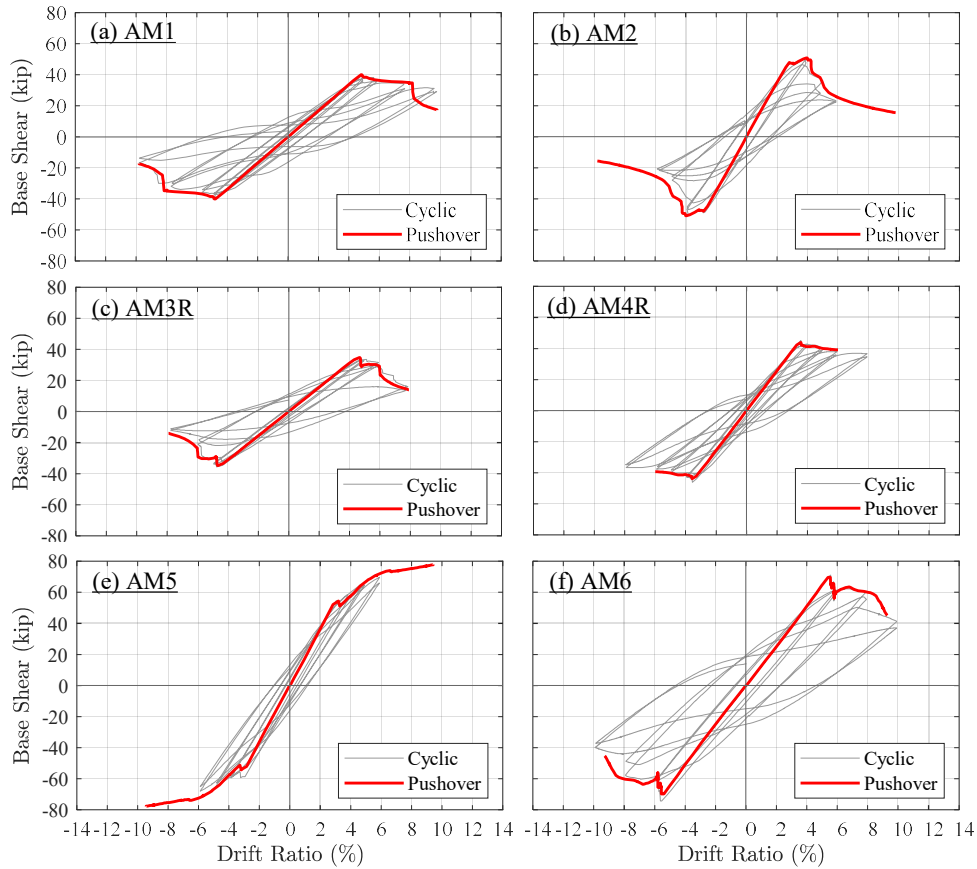


Figure 8. Quasi-cyclic and pushover response of archetypes [1kip = 4.448 kN].

4.4. Incremental Dynamic Analysis (IDA)

The objective of the non-linear incremental dynamic analysis (IDA) is to determine the ground motion intensity corresponding to the collapse of the structure, per the FEMA P695 procedure. A collapse limit (e.g., drift limit) is required in the IDA procedure to estimate the probability of collapse and determine the acceptability of the seismic response modification coefficients utilized in design. Selection of the collapse limit for the modular metal buildings requires some care. In the available full-scale (clear-span) metal building shake table tests (Uang et al., 2011; M. D. Smith, 2013) collapse was not observed up to 4% story drift, so a direct experimental collapse drift limit is unavailable. Moen et al. (2010) utilized a 4.5% collapse drift limit in their modeling, based on the observation that plastic strain accumulation in the rafter and panel zone would eventually lead to fracture (which was not included in the model). Modular metal building systems are flexible. Review of the pushover response of Figure 5 indicates that most of the archetypes are in the elastic or initial post-yield hardening response at 4.5% drift; therefore, such a limit for collapse would be inappropriate. An archetype dependent collapse drift limit is possible; however, a simpler approach was selected here – the collapse drift limit was assumed to be 6% for modular metal buildings. In all archetypes, except for AM2, the ultimate drift ratio (drift ratio corresponding to 20% strength loss) is greater than 6%. Plastic strain accumulation does not initiate until the first significant nonlinear response is observed, which is generally greater than 4% - thus the use of 6% recognizes the inherent flexibility of the modular metal building archetype, but still limits the total

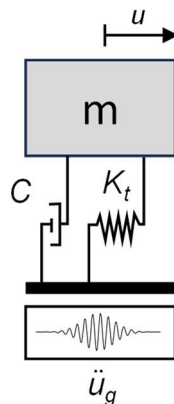
337 plastic strain accumulation in the response.

338 A set of 22 pairs of ground motions (44 total) specified in Appendix A of FEMA P695 were
339 used for the IDA. The IDA procedure starts by defining the median spectral intensity of the far-
340 field record set, S_T , measured at the fundamental period of the structure, and then the far-field
341 record set is scaled by $\alpha = S_{MT}/S_T$, where α is the intensity factor, and S_{MT} is the spectral intensity
342 corresponding to the maximum considered earthquake (MCE) at the fundamental period of the
343 structure. The median collapse intensity corresponding to the spectral acceleration at the
344 fundamental period of the building at which half of the ground motions cause collapse is referred
345 to as \hat{S}_{CT} . IDAs are performed using the nonlinear SDOF modeling protocol introduced in the
346 following section.

347 **4.4.1. Computationally Efficient Non-linear Dynamic Analysis Framework**

348 The dynamic behavior of metal buildings, as a single-story moment frame with roof masses,
349 can be represented by a single degree of freedom (SDOF) dynamic system. The first mode mass
350 participation ratio of previously studied clear-span metal buildings is between 76% and 83%
351 (Moen et al., 2019). The first mode mass participation ratio of the modular metal building
352 archetypes with 50 ft [15.2 m] modules (AM1 – AM4R) are between 92% and 99% per Table 5.
353 The longer span 100 ft [30.4 m] modules of AM5 and AM6 have lower mass participation ratios,
354 74% and 93% respectively. The long rafter spans and short columns of AM5 are indicative of the
355 potential for some higher mode response in this specific archetype; however, the nonlinear static
356 response and observed failure mechanism is benign in this archetype as indicated by its high
357 overstrength and ductility (see Figure 5 and Table 3) and the lower mass participation ratio for this
358 archetype was deemed acceptable for the study.

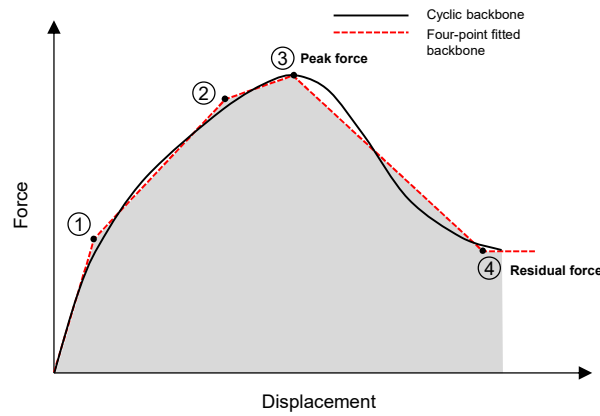
359 A classical SDOF dynamic model can be represented by a lumped mass, m , spring stiffness
360 K_t , and damping c , as shown in Figure 9. The dynamic properties, specifically the period of
361 vibration, T , can be selected so the SDOF model is consistent with what would be expected for the
362 actual building. Strength and stiffness degradation, and the period shift as the building experiences
363 damage during an earthquake are approximated by the nonlinear spring stiffness, K_t . A SDOF
364 hysteretic material model may be matched to the cyclic hysteretic response of the high-fidelity
365 model. With this high fidelity to SDOF mapping, the SDOF cyclic response includes local and
366 system-level responses, including rafter lateral-torsional buckling and local buckling and bracing
367 from the secondary structural system (purlins, girts, kickers, etc.).



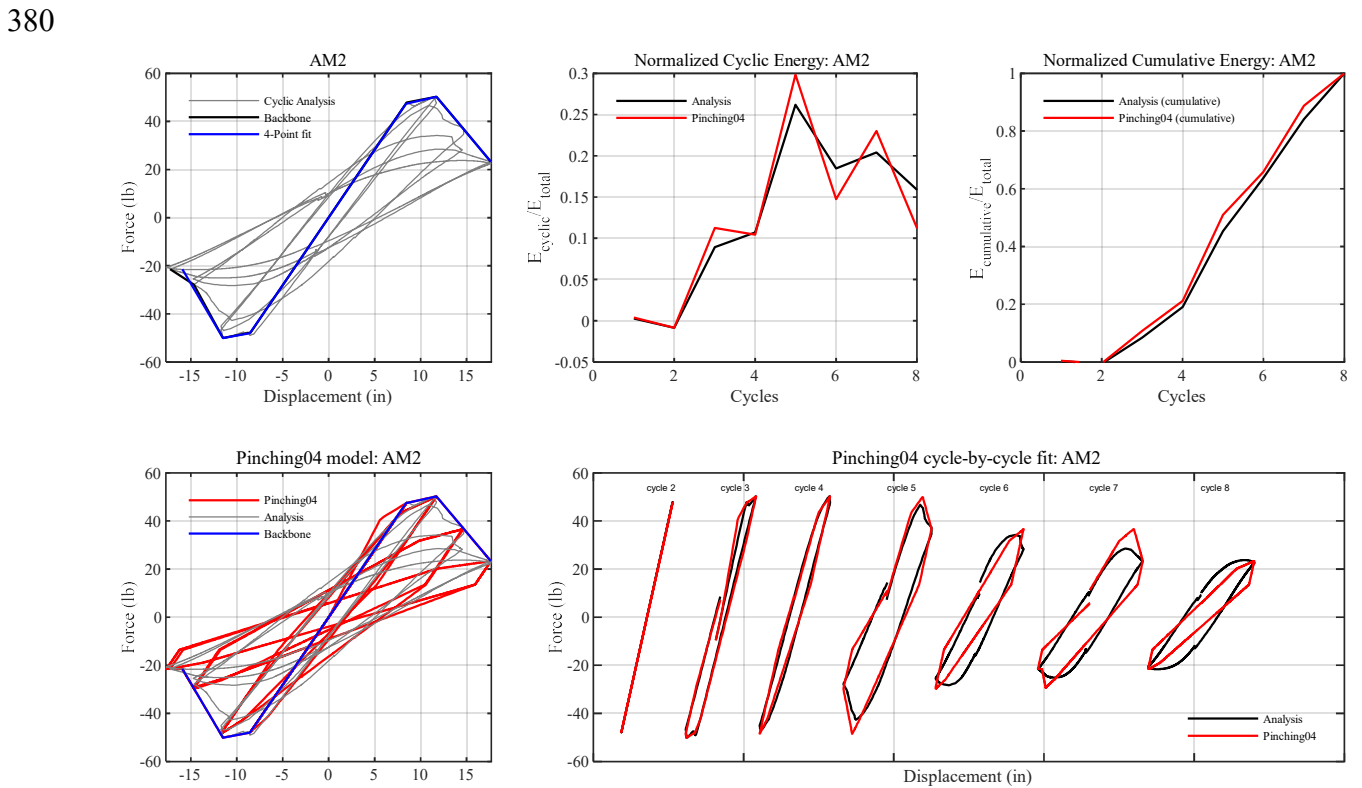
368
369

Figure 9. Metal building non-linear SDOF model definitions

370 The Pinching 04 material model in OpenSees is utilized for the nonlinear SDOF material
 371 hysteretic model. The Pinching 04 model includes the definition of four response points as
 372 illustrated in Figure 10 and additional parameters to handle loading/unloading (pinching) and
 373 cyclic degradation. Here the backbone points and other parameters are established such that the
 374 per cycle and accumulated error between the SDOF model and the high-fidelity model response
 375 are minimized as illustrated for AM2 in Figure 11. This process is repeated for all studied
 376 archetypes. The Pinching 04 model fitting parameters for all archetypes are presented in Table A
 377 of Appendix.



378 **Figure 10. A four-point backbone fitted to the cyclic backbone is shown in the first quadrant.**



381 **Figure 11. Quasi-static cyclic response of AM2 - high fidelity simulation and fitted response using**
 382 **Pinching 04 hysteretic model in OpenSees (McKenna et al., 2004) [1 kip = 4.448 kN; 1 in. = 25.4**
 383 **mm].**

385
386
387
388
389
390

The seismic mass, m , is assumed to be equal to the mass used to calculate the design seismic weight in an equivalent lateral force procedure. Matching the fundamental building period to the SDOF model is desirable so that elastic behavior and the natural periods are consistent. The relationship between the mass, initial stiffness, and the period of the building can be written as follows:

$$T_1 = 2\pi\sqrt{m/k_i} \quad (2)$$

391

392 where m is the seismic mass, k_i is the initial stiffness of the building in the SDOF model, and T_1
393 is the fundamental period of the SDOF model. Since the building period is determined by high-
394 fidelity analysis, and the seismic mass of the building is also defined in the seismic design of the
395 building, an equivalent initial stiffness is required to match the actual building period to the SDOF
396 model. FEMA P695 (Chapter 6) (ATC, 2009) addresses this challenge by defining an effective
397 yield roof drift displacement, $\delta_{y,eff}$, as defined in Eq. (1). For a single-story structure like a metal
398 building, the modal coefficient C_o is 1.0, and by assuming that the actual period of the building is
399 larger than the ASCE 7 (ASCE, 2010) prediction ($T_1 > T$), Eq. (1) can be simplified to:

$$V_{max}/\delta_{y,eff} = 4\pi^2 m/T_1^2 \quad (3)$$

400

401 By further noting $k_{eq} = V_{max}/\delta_{y,eff}$, the equivalent initial stiffness for the SDOF model, k_{eq} , can
402 be calculated as:

$$k_{eq} = 4\pi^2 m/T_1^2 \quad (4)$$

403

404 This equivalent initial stiffness is used in the Pinching 04 models.

405 The last term to consider in the SDOF dynamic equation is energy dissipation treated with the
406 viscous damping ratio, ξ . For all simulations in this study, $\xi=2\%$ is selected, corresponding to a
407 low-intensity elastic response, assuming that energy dissipation from yielding, buckling, and
408 damage is accounted for in the hysteretic response.

409

4.4.2. IDA and Fragility Curves

410 The IDA response: story drift vs. earthquake spectral acceleration scale factor and resulting
411 fragility response for all archetypes are provided in Figure 12(I) and (II), respectively. As an
412 example, for AM5, the median collapse capacity (from all 44 records) is $\hat{S}_{CT} = 0.75$ g (Figure 12(e)
413 (II)), and the $CMR = \hat{S}_{CT}/S_{MT} = 0.75/0.59 = 1.27$. Collapse fragility curves are also used to express
414 this information, where the cumulative collapse probability is related to the ground motion spectral
415 intensity. The discrete points in Figure 12 are obtained directly from the collapse points of the IDA
416 curve for each archetype. A lognormal distribution is fit to the data to get a smooth curve and
417 obtain \hat{S}_{CT} .

418
419
420
421

Per FEMA P695, the fragility response should be modified with the spectral shape factor, SSF ,
to account for the spectral shape. The SSF is a function of the building fundamental period, T , and
period-based ductility, μ_T , used to calculate the adjusted collapse margin ratio as $ACMR =$
 $SSF \times CMR$. For AM5, for example, $ACMR = 1.17 \times 1.27 = 1.48$. Similar results are provided for all

422 studied archetypes in Table 6.

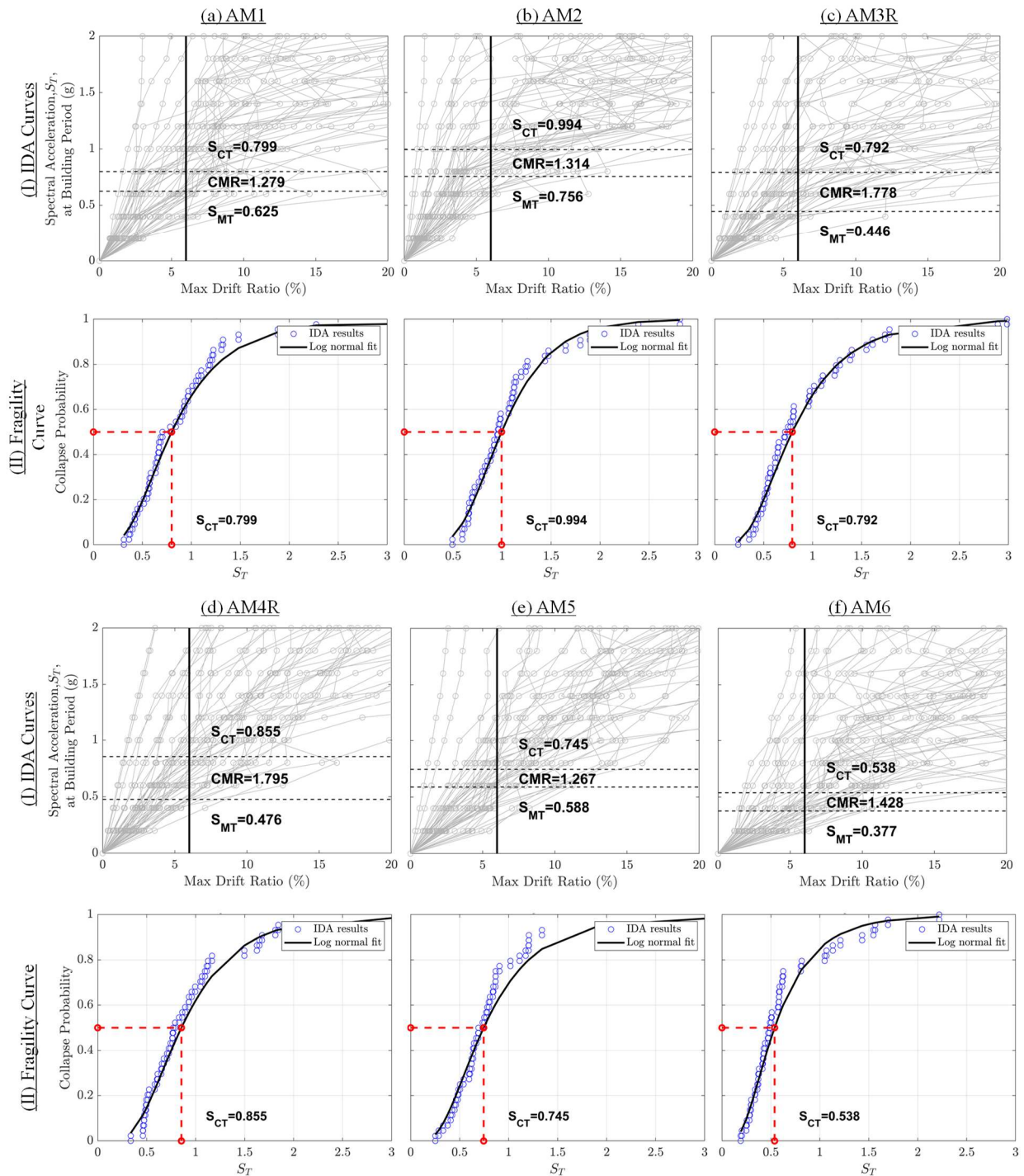


Figure 12. IDA and fragility curves for archetypes.

423
424

425 4.5. Seismic Performance Assessment per FEMA P695 Methodology

426 Per FEMA P695 (ATC, 2009), the performance of a system is judged by comparing the
 427 adjusted collapse margin ratios ($ACMR$) to the lower bound acceptable collapse margin ratios:
 428 $ACMR_{10\%}$ or $ACMR_{20\%}$ as specified in FEMA P695 (ATC, 2009). The performance of a structural

429 system is acceptable if, under the MCE ground motion, each archetype has a large enough collapse
 430 capacity such that the probability of collapse is less than 20% ($ACMR > ACMR_{20\%}$), and the
 431 performance group must, on average, have less than 10% probability of collapse ($\overline{ACMR} >$
 432 $ACMR_{10\%}$, where \overline{ACMR} is the average $ACMR$ of the performance group). The acceptable $ACMR$ s
 433 are calculated by assuming the distribution of collapse level spectral intensities is lognormal, with
 434 a median equal to \hat{S}_{CT} , and a standard deviation of β_{TOT} , which represents the total uncertainty in
 435 the collapse behavior of the system calculated as:

$$\beta_{TOT} = \sqrt{\beta_{RTR}^2 + \beta_{DR}^2 + \beta_{TD}^2 + \beta_{MDL}^2} \quad (5)$$

436

437 Where β_{RTR} is the record-to-record collapse uncertainty defined as:

$$\beta_{RTR} = 0.1 + 0.1\mu_T \leq 0.4 \quad (6)$$

438

439 β_{DR} reflects the uncertainty in the implementation of design and quality assurance
 440 requirements, β_{TD} demonstrates the uncertainty in the quality and completeness of the test data to
 441 characterize the structural behavior, and β_{MDL} reflects the uncertainty in the accuracy and
 442 variability of the structural modeling (ATC, 2009).

443 For the present study, β_{TOT} was defined using Eq. (5), and the assumed uncertainties were β_{DR}
 444 = 0.20, $\beta_{TD} = 0.20$, and $\beta_{MDL} = 0.10$. β_{DR} is low because the archetype buildings are designed
 445 professionally, and the designs are reviewed internally and by the MBMA seismic steering group.
 446 The test data-related uncertainty β_{TD} is low since shake table test data is available for the underlying
 447 modeling protocol development. The modeling-related uncertainty β_{MDL} is low because collapse
 448 characteristics, including local and global buckling, are represented well in high-fidelity and non-
 449 linear SDOF models.

450 The seismic response parameters, specifically, the median collapse intensity, \hat{S}_{CT} , the collapse
 451 margin ratio, CMR , the adjusted collapse margin ratio, $ACMR$, and acceptable collapse margin
 452 ratios ($AMCR_{10\%}$ and $AMCR_{20\%}$) are summarized in Table 6. The index archetypes meet the
 453 individual and group acceptance criteria. Thus, the assumed design seismic response modification
 454 factor $R = 3.5$ (Table 2) is deemed to satisfy the minimum acceptance criteria of FEMA P695
 455 (ATC, 2009) for modular metal buildings with two and three spans with different heights and span
 456 widths.

Table 6. Summary of archetypes analyses results: collapse drift limit of 6% ($R = 3.5$, $\Omega_o = 3$, $C_d = 3$)

Archetype	Ω_o	μ_T	S_{CT}	S_{MT}	CMR	SSF	$ACMR$	$ACMR_{10\%}$	$ACMR_{20\%}$	Check (Pass/Fail)
	(-)	(-)	(g)	(g)	(-)	(-)	(-)	(-)	(-)	
AM1	2.27	1.86	0.80	0.63	1.28	1.21	1.54	1.70	1.42	Pass
AM2	1.99	1.57	0.99	0.76	1.31	1.16	1.52	1.66	1.39	Pass
AM3R	1.87	1.47	0.79	0.45	1.78	1.16	2.07	1.65	1.39	Pass
AM4R	1.65	>1.98	0.85	0.48	1.79	1.23	2.20	1.72	1.43	Pass
AM5	2.28	>1.51	0.75	0.59	1.27	1.17	1.48	1.65	1.39	Pass
AM6	2.00	1.62	0.54	0.38	1.43	1.18	1.69	1.67	1.40	Pass
Average							1.75	1.67	-	Pass

5. DISCUSSION

High fidelity simulations coupled with surrogate models can provide an effective means for evaluating metal building system seismic performance. Conventional design processes provide acceptable outcomes in past experimental work and current P695-based modeling efforts, but may still behave differently than expected by engineers. Drift is driven largely by LTB between and across brace points, not yielding. Modifying R in the initial design does not typically result in significantly different frame performance given the limited range in which lateral loads control the moment envelope and that frames are fully optimized to that moment envelope. Lateral performance of the frames in modular metal buildings is not markedly different from clear-span buildings; however, they can be much more flexible. Innovative seismic systems and the necessity of the limits of current ASCE 7 code provisions (height, weight, etc.) could all now be efficiently explored using the developed models and protocols.

6. SUMMARY AND CONCLUSION

This study evaluated the seismic performance of modular metal buildings in high seismic zones using the FEMA P695 methodology. A representative set of archetype buildings, reflecting current industry design practices and incorporating Ordinary Moment Frame (OMF) behavior with a response modification factor of $R = 3.5$, was developed and analyzed through modal analysis, nonlinear static pushover, quasi-static cyclic simulations, and incremental dynamic analyses (IDAs). High-fidelity finite element models, calibrated to experimental data from prior shake table and subassembly tests, were used to capture the nonlinear behavior of the archetypes and to provide an accurate assessment of collapse performance.

The results of this study confirm that modular metal buildings designed with $R = 3.5$ can meet the FEMA P695 acceptance criteria, provided that lateral bracing systems for both columns and rafters are designed to satisfy the strength and stiffness requirements of AISC 360 Appendix 6. In contrast, buildings designed with traditional strength-only (2%) bracing methods exhibited reduced ductility and early onset of lateral-torsional buckling (LTB) in columns, which significantly compromised ductility. Redesign of the lateral bracing to include adequate stiffness, in accordance with AISC provisions, resulted in improved post-peak behavior and increased system ductility.

The nonlinear static and dynamic analyses also showed that modular metal buildings remain

488 largely elastic up to approximately 4% story drift and that ultimate drift ratios generally exceed
489 6%. Based on this observed performance, a collapse drift limit of 6% is proposed as more
490 appropriate for modular metal buildings than the 4.5% previously adopted in studies of clear-span
491 metal buildings. The calibrated single-degree-of-freedom (SDOF) models used in this study were
492 able to effectively reproduce the cyclic and collapse behavior of the archetypes, enabling efficient
493 implementation of the FEMA P695 framework.

494 Overall, the results confirm the applicability and adequacy of the ASCE 7 seismic design
495 provisions where modular metal buildings are categorized as Ordinary Moment Frames, when
496 modern bracing design practices are employed. The study highlights the importance of meeting
497 both strength and stiffness criteria in lateral bracing systems, and provides a technical foundation
498 for the continued use of $R = 3.5$ in the seismic design of modular metal buildings.

499 **7. ACKNOWLEDGMENTS**

500 The authors would like to thank the Metal Building Manufacturers Association (MBMA)
501 Seismic Research Steering Group who provided thoughtful advice, input, effort, and feedback
502 throughout this project. In addition, several engineers in this group provided the complete designs
503 for the metal building system archetypes. The authors would also like to thank the peer review
504 panel comprised of Dr. Greg Deierlein, Dr. Michael Engelhardt, and Dr. Tom Sabol who reviewed
505 the modeling protocols and conclusions in detail for the clear-span seismic study that preceded
506 this work. In addition, Dr. Chia-Ming Uang was gracious with his time and data during the
507 validation phase of the modeling. Finally, Dr. Lee Shoemaker and Mr. Vincent Sagan of MBMA
508 were instrumental in shepherding this project to a meaningful end. The team would also like to
509 recognize the financial support of MBMA in conducting the work.

510

511 **8. REFERENCES**

- 512 AISC. (2010). *ANSI/AISC 341-10, Seismic Provisions for Structural Steel Buildings*.
513 American Institute of Steel Construction.
- 514 AISC. (2016). *ANSI/AISC 360-16, Specification for Structural Steel Buildings*. American
515 Institute of Steel Construction.
- 516 ASCE. (2016). *Minimum Design Loads for Buildings and Other Structures*. American
517 Society of Civil Engineers.
- 518 ATC. (2009). *Quantification of Building Seismic Performance Factors* (Issue FEMA-P695).
- 519 Bagatini Cachuco, F. (2021). *Seismic Performance Evaluation of Steel Building Systems in*
520 *Canada*. University of British Columbia.
- 521 Bagatini Cachuco, F., & Yang, T. Y. (2021). Seismic performance assessment of pre-
522 engineered steel buildings on the west coast of Canada. *Steel and Composite Structures,*
523 *An International Journal*, 41(3), 461–474.
- 524 Hong, J. K., & Uang, C. M. (2006). *Cyclic performance evaluation of a metal building system*
525 *with web-tapered members*. Report No. SSRP-06.
- 526 Jerry Hatch. (2014, August). New Advances in Design and Testing for Seismic Demands.
527 *STRUCTURE*.

528 Kaehler, R. C., White, D. W., & Kim, Y. D. (2011). *Frame design using web-tapered*
529 *members*. American Institute of Steel Construction Chicago, IL, USA.

530 Kim, Y. D. (2010). *Behavior and Design of Metal Building Frames with General Prismatic*
531 *and Web-Tapered Steel I-Section Members*. School of Civil and Environmental
532 Engineering, Georgia Institute of Technology.

533 McKenna, F., Fenves, G. L., & Scott, M. H. (2004). *Open System for Earthquake Engineering*
534 *Simulation*.

535 Meimand, V., Moen, C., & Schafer, B. (2018). Examination of Seismic Response
536 Modification Coefficients for Metal Building Systems with FEMA P695 Process.
537 *Proceedings of the 11th National Conference in Earthquake Engineering*.

538 Moen, C. D., Torabian, S., & Schafer, B. W. (2019). *Evaluation of Metal Building System*
539 *Seismic Response Modification Coefficients*.
540 <https://jscholarship.library.jhu.edu/items/3fb18f3a-c7e9-4696-b32a-188fd336af76>

541 Prawel, S. P., Morrell, M. L., & Lee, G. C. (1974). Bending and buckling strength of tapered
542 structural members. *Welding Research Supplement*, 53(February), 75–84.

543 Schafer, B. W., Li, Z., & Moen, C. D. (2010). Computational modeling of cold-formed steel.
544 *Thin-Walled Structures*, 48(10–11), 752–762.

545 Simulia. (2014). *ABAQUS Version 6.14*.

546 Smith, M. D. (2013). *Seismic testing and analytical studies for the development of new*
547 *seismic force resisting systems for metal buildings*. Ph.D Dissertation, University of
548 California, San Diego.

549 Smith, M. D., Turner, K. T., & Uang, C. M. (2013). *Experimental Investigation of Cyclic*
550 *Lateral Buckling of Web-Tapered I-Beams*. Report No. SSRP-12.

551 Uang, C. M., Smith, M. D., & Shoemaker, W. L. (2011). Earthquake simulator testing of
552 metal building systems. *Structures Congress 2011*, 693–704.

553

554

555 9. APPENDIX

556

Table A. Pinching 04 model parameters for all archetypes

Parameter	Unit	Archetype					
		AM1	AM2	AM3R	AM4R	AM5	AM6
ePf1	(kips)	23.6	29.4	17.4	27.1	41.8	43.2
ePd1	(in)	8.6	5.2	12.2	11.4	6.9	18.4
ePf2	(kips)	31.6	47.4	30.6	36.1	58.5	56.5
ePd2	(in)	11.6	8.4	21.6	15.2	10.9	24.0
ePf3	(kips)	39.4	50.2	35.1	45.1	69.7	71.1
ePd3	(in)	14.6	11.7	25.5	19.3	17.7	30.0
ePf4	(kips)	31.2	23.3	16.0	36.7	50.0	41.4
ePd4	(in)	26.7	17.6	43.6	35.3	20.0	54.7

eNf1	(kips)	-24.1	-26.3	-21.5	-29.4	-29.9	-44.7
eNd1	(in)	-8.8	-4.7	-15.0	-12.3	-4.9	-18.9
eNf2	(kips)	-28.8	-48.0	-28.4	-35.6	-60.6	-56.0
eNd2	(in)	-10.5	-8.6	-19.8	-15.0	-10.0	-23.7
eNf3	(kips)	-39.6	-50.1	-35.6	-46.0	-67.9	-74.4
eNd3	(in)	-14.2	-11.5	-25.6	-19.2	-17.7	-30.4
eNf4	(kips)	-16.7	-21.5	-12.1	-36.6	-50.0	-39.9
eNd4	(in)	-30.7	-15.9	-38.4	-32.6	-20.0	-53.8
rDispP	(-)	0.705	0.667	0.648	0.751	0.656	0.533
rForceP	(-)	0.917	0.863	0.857	0.834	0.757	0.979
uForceP	(-)	-0.615	-0.581	-0.564	-0.585	-0.617	-0.514
rDispN	(-)	0.603	0.789	0.810	0.797	0.625	0.799
rForceN	(-)	0.934	0.877	0.877	0.835	0.763	0.982
uForceN	(-)	-0.638	-0.631	-0.629	-0.609	-0.608	-0.631
dmgType	(-)	energy	energy	energy	energy	energy	energy

557